



SEGMENTATION AND PRE-PROCESSING OF INTERSTITIAL LUNG DISEASE USING DEEP LEARNING MODEL

PRIYANKA YADLAPALLI *AND D. BHAVANA †

Abstract. Medical image processing involves using and examining 3D human body images, which are most frequently acquired through a computed tomography scanner, to diagnose disorders. Medical image processing helps radiologists, engineers, and clinicians better comprehend the anatomy of specific patients or groups of patients. Due to recent advancements in deep learning techniques, the study of medical image analysis is now a quickly expanding area of research. Interstitial Lung Disease is a chronic lung disease that worsens with time. This condition cannot be completely treated when the lungs have been damaged. Early detection, on the other hand, aids in the control of the disease. It causes lung scarring as a result. The first methodology characterizes lung tissue utilizing first order statistics, grey level occurrence, run length matrices, and fractal analysis. It was suggested by Uppaluri et al in one instance. In the pre-processing step, patients' CT scans are presented using various color map models for better understanding of data-set, and also for determining the patients final Force Vital Capacity and Confidence values using a Pytorch model with leaky relu activation function. These variables can be used to determine whether a person has a disease. Segmentation is a crucial stage in employing a computer assisted diagnosis system to estimate interstitial lung disease. Accurate segmentation of aberrant lung is essential for a trustworthy computer-aided illness diagnosis. Using separate training, validation, and test sets, we proposed an efficient deep learning model using Unet architecture and Densenet121 to segment lungs with Interstitial Lung Disease. The proposed segmentation model distinguishes the exact lung region from the ct slice background. To train and evaluate the algorithm, 176 sparsely annotated Computed Tomography scans were utilized. The training was completed in a supervised and end to end manner. Contrary to current approaches, the suggested method yields accurate segmentation results without the requirement for re-initialization. We were able to achieve an accuracy of 92.59 percent after training the proposed model with Nvidia's CUDA GPU.

Key words: Medical Image Processing, Interstitial Lung Disease, Force Vital Capacity, Pytorch, Densenet121

AMS subject classifications. 68T05

1. Introduction. Deep learning is a component of machine learning, an artificial intelligence subset. Broadly speaking, "artificial intelligence" refers to techniques that enable computers to mimic human behaviour. All of this is made possible through machine learning, which consists of a collection of algorithms that are taught using data. A subset of machine learning called "Deep Learning" is inspired by the structure of the human brain. Deep Learning systems continuously analyse data using a predetermined logical framework in an effort to make decisions that are comparable to those made by humans. To accomplish this, deep learning uses neural networks, a multi-layered architecture of algorithms. Advances in deep learning for medical image analysis have created new opportunities for morphological and textural pattern discovery in images using only data [2].

Deep learning models can fix issues that machine learning models cannot is shown in Fig.1.1. and deep learning has been given credit for all recent developments in artificial intelligence. There would be no self-driving cars or personal assistants like Alexa and Siri without deep learning. The Google Translate app wouldn't have changed from 10 years ago, and neither Netflix nor Youtube would know what movies or TV shows we enjoy or dislike. These developments are all driven by neural networks. Processing power is required for deep learning in a substantial way. High performance graphics processing units (GPUs) are appropriate since they have a lot of memory and can do a lot of tasks over multiple cores. On-premises management of several GPUs, however, can put a heavy burden on internal resources and be prohibitively expensive to scale

*Asst. Professor, Department of ECE, GRIET Hyderabad, Telangana, India (bhavanaece@kluniversity.in)

†Department of Electronics and Communication Engineering, Koneru Lakshmaiah Education Foundation, Guntur District, AP 522502, India (bhavanaece@kluniversity.in)

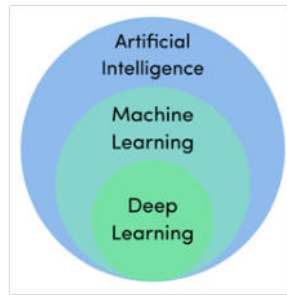


Fig. 1.1: Deep Learning

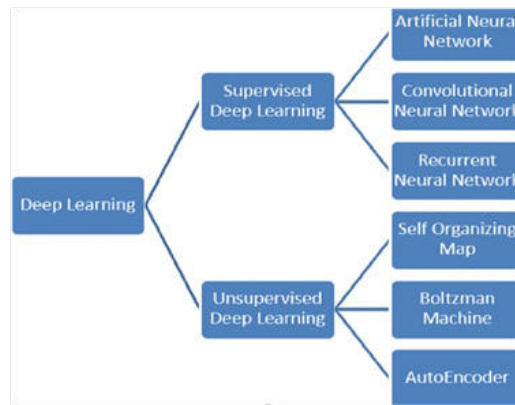


Fig. 1.2: Types of Deep Learning Algorithms

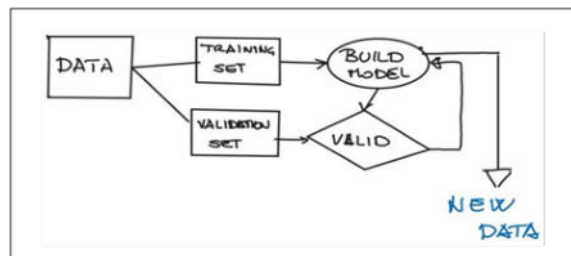


Fig. 1.3: Supervised Learning Algorithm

1.1. Deep Learning Algorithms. Deep learning algorithms are dynamically constructed to run over numerous layers of neural networks, which are simply a collection of pre-trained decision-making networks. Each of them is then processed through a series of simple layered representations before being moved to the next layer.

The most popular type of Deep Learning is Supervised Learning. During the training phase of supervised learning, a set of examples, known as training set, is submitted as input to the system. Each input is tagged with a desired output value, so the system understands what the output should be when the input is given. The brief classification of deep learning algorithms is shown in Fig.1.2.

Supervised learning shown in Fig.1.3 is the most common type of Deep Learning.

1. A set of examples known as the training set is submitted to the system as input during the training

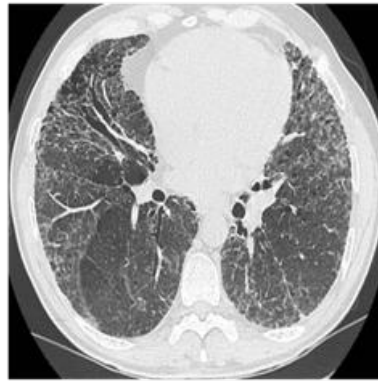


Fig. 2.1: Lung effected with ILD

phase of supervised learning

2. Each input is labelled with a desired output value so that the system knows what to expect when the input is given

2. Interstitial Lung Disease (ILD). Several disorders that result in scarring in the lungs are referred to together as "interstitial lung disease" (ILD). It is also known by the name diffuse parenchymal lung disorders. Scarring causes stiffness in the lungs, making it difficult to breathe and supply oxygen to the circulation. ILDs result in permanent lung damage that develops over time. Medication can help to delay the progression of interstitial lung disease, but many people never fully restore their lung functions [3].

The different types of Interstitial Lung Disease includes Mycoplasma pneumonia, Asbestosis, Acute interstitial pneumonitis, Hypersensitivity pneumonitis. Inhaling asbestos, a fibre which is present in building materials, can result in asbestosis, a kind of interstitial lung disease shown in Fig.2.1. Acute interstitial pneumonitis is caused due to rapidly progressive dyspnoea which can be developed from days to weeks . Hypersensitivity pneumonitis is the medical term for the condition that occurs while breathing in dust, mould, or other irritants over an extended period of time. The symptoms are: shortness of breath at rest or when exercised, cough that isn't watery, fatigue, unintentional weightloss, clubbing of fingernails and toes, pain in joints and muscles. After an injury, an abnormal healing reaction in the lungs appears to be the origin of interstitial lung disease. Our body typically produces just enough new tissues to correct the existing damage. When the repair system malfunctions in interstitial lung disease, the tissue that surrounds the air sacs gets scars and thickens. This complicates the flow of oxygen into your bloodstream. Long-term exposure to chemicals and pollution can harm your lungs. Examples include silica dust, asbestos fibres, grain dust, coal dust, and radiation treatments (lung or breast cancer). Interpretation of ILD and other lung illnesses is made simpler by the accurate view of lungs blood vessels and tissues [4]. Hence Such anomalies are frequently found using computer aided diagnosis methods [5].

Segmentation techniques shown in Fig.2.2 that were manual or semiautomatic in early CAD systems are now replaced by completely automatic segmentation algorithms. A local texture classification algorithm that goes across images and generates a map of diseases has typically been used to diagnose ILDs. Deep artificial neural networks and deep convolution neural networks have recently received a lot of interest following their outstanding performances in the Image-net Large Scale Visual Recognition Competition in 2012 [6]. These networks have been around for a while, but only recently have they been able to perform well, in large part because of the abundance of annotated data accessible, the extreme parallelism power of GPU, and a few clever design choices [7]. Recent research has also looked into the potential advantages of deep learning algorithms for medical picture processing, and the preliminary findings are encouraging [8].

2.1. Segmentation. Segmenting the lungs is a particularly tough task due to in homogeneities in the lung region and pulmonary structures with similar densities, such as arteries and veins. Several segmentation approaches have been put out in the past. These methods can be broadly categorised as rule based, knowledge

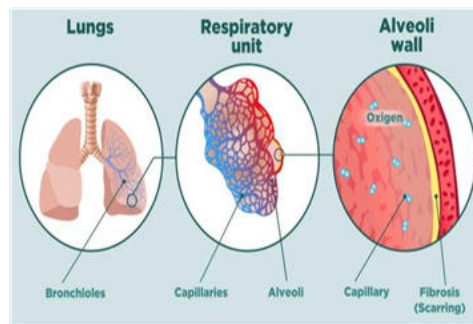


Fig. 2.2: Dissection of ILD Lung consisting of Scarring

based, pixel based, texture analysis based, and model based. Shanhui Sun and Geoffrey McLennan's [9] rule-based technique of lung segmentation identifies potential airways before applying rules to determine the lungs.

Benefits of segmentation:

1. Image segmentation is the most important medical imaging process. It uses an automatic process to extract the ROI (region of interest). Segmentation divides an image into areas of interest, such as body organs or tissue.
2. Application of classification neural network algorithms to segmented radiological images can significantly improve segmentation accuracy.
3. While manual segmentation increases computational costs, but it significantly reduces overall disease diagnosis costs.

3. Related Work. Computer aided diagnostic analysis is necessary for treatment planning, tracking the course of illness of a diseases, identifying how well a patient responds to a prescribed medication, and other purposes. Medical image modalities create images using a range of techniques for a variety of objectives. Hamzah and Mohd Faizal Mohd present a novel method for diagnosing interstitial lung disease (ILD) using high resolution computed tomography images and correlation and regression algorithms on texture measure [10]. This study predicts each patient's final FVC measurements and provides a Confidence value so that different Machine Learning models can be compared and contrasted [11].

A Convolutional Neural Network (CNN) was used to classify 2D lung images as part of a novel approach for diagnosing interstitial lung disease. The suggested method obtained 94 percent accuracy and high sensitivity on a dataset of 30 CT scan images. The same dataset was classified with an accuracy of 86% using the SVM classifier [12].

In order to identify ground glass opacities (GGO) on HRCT, K.R. Heitmann and associates used neural networks and expert rules. To identify GGO in this work, a hybrid model made up of three single nets and an expert rule was constructed [13]. In order to create a consensus categorization for the entire group of IIPs (Idiopathic Interstitial Pneumonias), the American Thoracic Society (ATS) and the European Respiratory Society (ERS) worked together (ERS)[14]. It comprises classifications and definitions for clinical, radiological, and pathological conditions.

A computer-aided detection method for ILD patterns was developed by Y. Xu et al. using volumetric data from MDCT images. The most popular classifiers were Bayesian and SVM [15]. Using a multi-detector computed tomography (MDCT) dataset, Panayiotis D. Korfiatis looked into an automated technique for volumetric estimate of interstitial pneumonia patterns. The vascular tree volume and lung categorization were produced using 3D automated grey level thresholding with edge highlighting wavelet preprocessing. Then, for classification, the 3-class pattern categorization of the LP (lung parenchyma) is used [16]. For the categorization of emphysema in CT images of the lungs, Mardad.J.Ganes proposed a Textron-based classification strategy based on raw pixel representation with radial basis function kernel [17].

Rui Xu developed a method for recognising lung textural patterns using various expressions. The CT and eigenvalues of the Hessain matrices are used in this procedure [18]. For the classification of lung tissue

pattern, Adrien Depeursinge proposed near-affine-invariant texture descriptors derived from isotropic wavelet frames [19].

Jesus Loarce-Martos, Francisco Xavier Leon-Roman, and Sandra Garrote-Corral talked on improvements in home spirometry and quantitative computer tomography for the diagnosis and treatment of interstitial lung illness linked to connective tissue diseases [20]. Aasia Rehman, Dr. Majid Zaman, and Dr. Muheet Ahmed Butt reported a range of medical imaging methods in their survey[21] Panfang Hua's [22] region growth approach is unreliable in high attenuation patterns like ILD, but it performs well in the presence of noise and can correctly distinguish areas with the same properties. Azar Tolouee devised a threshold method that chooses the best threshold to distinguish the lung region from the backdrop [23]. It was discovered to be quite complex for ILD and missing several typical lung features. The fuzzy method is used for segmentation by M.Gomathi and P.Thangaraj [24], which takes less time between iterations to obtain the overall optimal solution but is unable to separate images corrupted by noise, outliers, and other artefacts. The diseases can be easily segmented with improved precision using the registration method for the lungs proposed by I. Sluimer [25]; however, the highest border placement error may occur and is only applicable in clinical practice

3.1. Dataset. Kaggle is a subsidiary of Google Limited Liability Company, which describes itself as "the home of data science." Experts in machine learning and deep learning can get together on the site. In 2010, Anthony Goldbloom and Ben Hamner launched this public data platform. San Francisco, California is the headquarters of the corporation. In a web-based data science environment, data scientists can use the kaggle platform to not only explore but also build models. We used a CT value thresholding technique to first estimate the size of the lungs and to identify normal and mild ILD lung parenchyma, which we then used to segment the lungs. Afterward, we further identified aberrant lung areas with severe ILD using texture-feature images produced from the co-occurrence matrix. Last but not least, we generated the final lung segmentation result by combining the initial lungs with the aberrant lung regions that were discovered. Following preprocessing, the datasets were divided at random into training and test sets, with 80% of the training data used to provide the segmentation models with knowledge about lung segments. Using the remaining 20% of the data, the segmentation models were evaluated. The model is trained using the train folder in order to achieve great efficiency and accuracy. After training the model, the test folder is used to observe the output in predicting the disease of the patient. In order to predict ILD in a patient, we employed the term FVC. The ratio of the lung's forced vital capacity to its forced expiratory volume in the first second is known as the FEV1/FVC. FEV1 is calculated as $A \times FVC + C$, where A is 0.84 and C is 0.23 FVC is calculated by using spirometry, which refers to how much air can be forcibly evacuated from your lungs after taking the deepest inhale possible. A patient's FVC is evaluated at each visit, and over the course of 1-2 years, numerous follow-up visits and a photo at Week 0 are all required. The train dataset contained a complete history of measurements as well as an anonymized computed tomography scan. The only tests included in the bundle are a baseline CT scan and a Forced Vital Capacity assessment. The following variables are included in the dataset: FVC is the measured lung capacity in millilitres; weeks denotes the number of weeks preceding/following the baseline CT; patient is a unique identifier for each patient; and percent is a calculated field that displays the patient's FVC as a percentage of the typical FVC for patients with comparable features.

4. Materials and Methods. For this study, we used a Chest CT-Scan image collection from the kaggle platform. Since CNN models may be trained on X-ray images in DICOM and JPEG formats[26-27], the X-ray images from two different kaggle datasets were first converted to PNG format. Given that the two datasets had different sizes, scaling the images was the next step towards standardisation. U-Net and DenseNet 121 in this study were built with 512 x 512 pixels because the input size for various convolutional architectures vary. Deep learning algorithms have often prioritized one of the two, rather than both usability and performance. A machine learning library called Pytorch shows how these two objectives may coexist by allowing code to be used as a model, streamlining debugging, and being compatible with many well-known computing libraries. It also manages to be effective and support hardware accelerators like GPUs. Performing pulmonary function testing on individuals with ILD is difficult during the present SARS-CoV-2 outbreak[28]. Specialists have advocated spirometry and video consultations at home. In recent years, home spirometry is often used to monitor the severity of ILD. Previous research has shown that daily home spirometry can be an effective method for tracking the progression of ILD. Furthermore, it provides essential clinical data and is clear enough for the majority of

patients to make the diagnosis.

4.1. Exploratory Data Analysis (EDA). An approach to data analysis called exploratory data analysis which uses data visualisation to examine and summarise data sets. It helps us figure out how to effectively manipulate data sources to get the results we're after, making it straightforward to identify trends, assess hypotheses, and confirm assumptions. EDA is frequently used in addition to formal modelling[29] to explore what information data might reveal and to better understand the features of data sets and how they relate to one another. During the data discovery stage, EDA approaches, created in the 1970s by American mathematician John Tukey, are still often utilised. In our experiment, we used the Laplace distribution to analyse the correlation between various variables in the supplied dataset and produced graphs for the same. The analytical functions and approaches that EDA tools could conduct are as follows:

1. Dimensional reduction and grouping techniques make it easier to create graphical representations of multivariate, and high-dimensional data
2. Summary statistics and a univariate visualization[30-31] are provided for each field in the raw dataset, We can assess the relationship between the variables in the dataset and the variable of interest using bivariate visualisations and summary statistics. Multivariate visualisations are used to depict and comprehend the relationships between several data categories.
3. K-means data points are divided into K groups according to how far away from the centroid of each group they are, using the unsupervised machine learning clustering process known as clustering. The data points that are grouped together are those that are closest to a given centroid. Clustering is used in K-means market segmentation, pattern detection, and image compression.
4. Predictive models, such as linear regression, create predictions about the future using statistics and data.

4.2. Augmentations. A computer vision technique called augmentations enhances the performance of deep convolutional neural networks. The library is useful for business, deep learning research, and machine learning competitions. Augmentations is a Python package that allows you to make quick and versatile image enhancements. Augmentations provides a simple, yet effective photo augmentation interface for a variety of computer vision applications such as object classification, segmentation, and detection. Augmentations works with a variety of data types, including photographs, medical imaging, satellite imagery, manufacturing and industrial applications, and generative adversarial networks. It operates quickly. Pytorch and Tensor Flow,[33] two deep learning frameworks, are supported.

4.3. Segmentation. Segmentation aids in determining where objects of various kinds appear in an image. U-Net is just a convolutional neural network structure which grew from the CNN design[34] with little alterations. It was created to deal with medical photographs with the goal of segmenting or classifying the affected body part.

4.3.1. U-Net Architecture. For all the biomedical image segmentation and other image transformation applications, the U-Net is a CNN architecture which is used. Due to its top class performance with less input, U-Net beats other convolutional models in pixel-based image segmentation. Fig.4.1 explains about U-Net architecture This unique model was constructed by Olal & Ronneberger et al. Model architecture for U-Net: There are two approaches which are present in U-Net architecture for segmenting biomedical pictures. The initial approach which is also known as encoder shortens. Context is captured by the encoder using a small feature map [35-37]. Max-pooling and convolution layers like Vgg-16 make up the encoder. The other half of the structure is made up of a uniform expanding path, also referred to as a decoder. The second path uses transposed convolution to perform the precise localization. The encoder section is comprised of numerous contraction blocks. The encoder adheres to ConvNet's traditional architecture. For contraction, the network employs a repeated implementation of two 3x 3 convolutions (ReLU) and a 2 x2 max-pooling operation with stride 2. The number of feature channels doubles with each downsampling step. The extensive path consists of upsampling a feature map, a 2 x 2 convolution ("up-convolution") that reduces the number of feature channels in half, concatenation with the equivalent feature map from the skip connection, two 3 x 3 convolutions, and two ReLUs. The component feature vector is mapped using a 1x 1 convolution at the top layer. There are a total of 23 convolutional layers in the network.

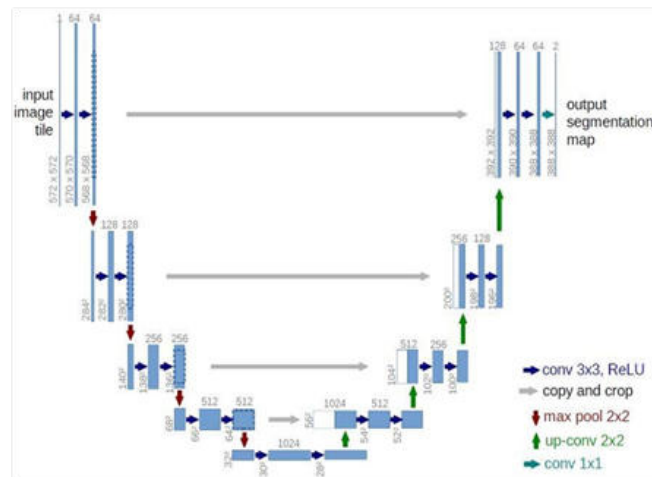


Fig. 4.1: Unet Architecture

4.3.2. Densenet121. As an encoder in our U-Net network, we used relatively simple CNN of DenseNet family. It is made up of four dense blocks with a transition layer between each pair in Fig.4.2. Each dense block has multiple convolution layers, and each transition layer has a batch normalisation, convolution, and average pooling layer. To boost nonlinearity DenseNet employs the activation function of ReLU.

Each layer of the convolutional neural network known as DenseNet shown in Fig. 4.2 is connected to every layer below it. When the composite function operation is applied, the output of the first layer becomes an input for second layer. The convolution layer, pooling layer, batch normalisation layer, and non-linear activation layer make up this composite process [38]. Densenet resolves the vanishing gradient problem, permitting the model to be trained with fewer features [39-40].

The densenet121 is: $5 + (6+12+24+16)*2 = 121$

- 5 – Convolution and pooling layers
- 3 – Transition layers (6,12,24)
- 1 – Classification layer (16)
- 2 – Dense block (1*1 and 3*3 Conv)

4.3.3. Imagenet. The ImageNet project is a sizable visual database that was developed to assist in the creation of software for visual object recognition. ImageNet is a massive image database with about 14 million images in it. The management category organises and labels photos. Machine Learning and Neural Learning Networks use a big database of images to teach machines. To learn useful aspects from these training photos, we need special equipment. As a result, ImageNet features a well-organized management board that makes it suitable for supervised machine learning. ImageNet is used to import the standard weights between the inputs, hidden, and output layers in a neural network. ImageNet is a massive image database with about 14 million images in it. ImageNet is used to import the standard weights between the inputs, hidden, and output layers in a neural network

4.3.4. Learning Rate. The learning rate is the time it takes for the upgrading steps to proceed across the gradient. The Learning rate parameter aids in the updating of the gradient, with a maximum value of 1 but typically a relatively low value. Consider the analogy of a rolling ball to better comprehend the learning rate. The learning rate can be calculated using this analogy by computing the discrete steps that are not continuous.

When it comes to training a network, the Learning rate parameter Fig. 4.3 is quite important. Even when the ball is in the line of sight, there will be little development if a slow learning rate is taken into account. However, if the ball is stuck in the local minima, it has a good chance of not reaching the global minima. The

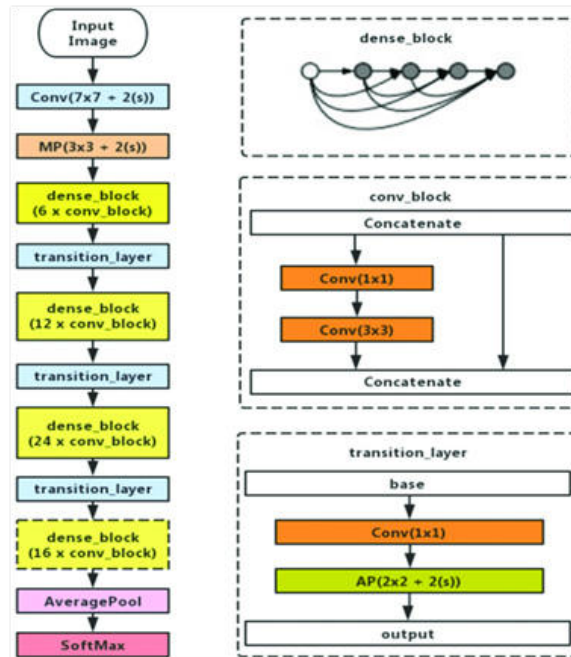


Fig. 4.2: Densenet121 Architecture

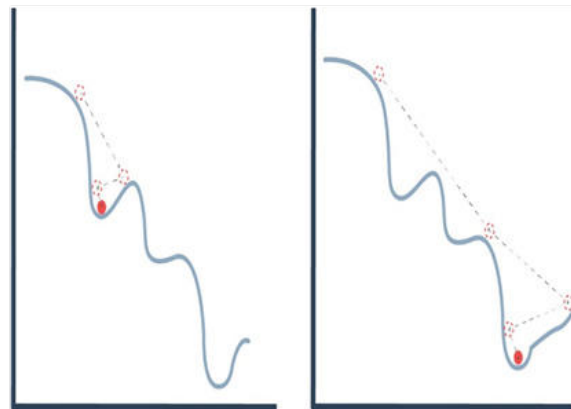


Fig. 4.3: Learning Rate (X-axis: Weight, Y-axis: Loss)

exact optima of the loss function can be attained by adjusting the precise learning rate. There are two ways to accomplish this. There are both greater and smaller steps. For every iteration, when there is a larger difference in weights it is considered as larger steps. In this method, the optimal result can be achieved in very little time, but the exact optimal value cannot be achieved. For every iteration, when there is a smaller difference in weights it is considered as smaller steps. In this method, there is a need for more epochs to get the optimal result, but they are very few chances to miss the exact optimal value

4.3.5. Early Stopping. Keras provides a function `EarlyStopping()`. It helps us to monitor the epochs and once set off it breaks the training. This callback is works when arguments are intialised. The monitor helps us to state the functioning and monitor and to stop the training. Calculation measurements on the test data

has prefix as $val_{eg} : val_{loss}$ for the loss on the test data. “mode” can be adjusted to either based on the use of metric which is selected if we want to increment then use maximize or max, if we want to decrement then use minimum or min.

Usually we use minimum validation loss and maximum val_{acc} . The default mode is “auto” which means to decrement the loss or increment the accuracy. Training will get to halt when the selected metric fails to perform better. For knowing which epoch the training has halted, “verbose” is set to 1. This will help us in printing the epoch. At initial sight if there is no improvement, this is not the suitable time for stopping the training as there are some models they get slightly worse or they shows no improvement prior to becoming better. This is performed by “patience” parameter Even if there is a small difference in performance metrics event it is still considered improvement. But if we want to consider it as improvement after a specific improvement that can be done using “min delta” parameter. We can to break the training if metric stays below or above a described verge. This can be done using baseline parameter

4.3.6. ModelCheckpoint. A checkpoint is an intermediary dump of internal state of entire model So when the Early Stopping halts epochs and when metrics are not satisfied even after training the model might not perform with its top accuracy on test data An extra function called Model Check Point () is used to store better ones for the whole observation in training and to use later. This is malleable and it is used in this scenario we will be using it to store better architecture identified throughout the learning. This can be obtained using the pip installer. This function saves model to the respective file. The path and file is mentioned in argument. Monitor argument helps us to monitor the loss function. We mention “mode” as min or max the measurement based on requirement. The mode of standard measure is defaultly set to “auto”. We need suitable model throughout the learning. This is achieved by giving save_best_only parameter as True. If we want to know at which epoch model was saved or check the performance measure we set verbose as “1” in callback:

ModelCheckpoint('best_lung_unet_densenet121.h5',mode='min', monitor='val_loss', verbose=1).

load_model() is used to load and evaluate the saved model any time.

4.3.7. Proposed model. In addition to providing the final FVC values and their corresponding confidence values, we proposed a Pytorch model for identifying ILD. The results of a spirometer, which measures the amount of air breathed in and out, will be used to assess lung function, and a CT scan of the patient’s lungs will be used to estimate the extent of the patient’s loss of lung function. All patients’ initial confidence intervals are set at 100. The FVC test gauges a patient’s capacity to forcefully and swiftly expel air after taking a deep breath. The lung volume is expressed in milliliters. The improvement in FVC over a few weeks is used to forecast the patient’s decline in lung function. The results of a spirometer, which measures the amount of air breathed in and out, will be used to assess lung function, and a CT scan of the patient’s lungs will be used to estimate the extent of the patient’s loss of lung function. All patients’ initial confidence intervals are set at 100. The FVC test gauges a patient’s capacity to forcefully and swiftly expel air after taking a deep breath. The lung volume is expressed in milliliters. The improvement in FVC over a few weeks is used to forecast the patient’s decline in lung function. For a variety of reasons, some individuals may not have improved or not sufficiently responded to treatments. Since their FVC improves steadily and with few peaks and valleys, some people, on either side, are definitely improving. Patients with those traits are incredibly uncommon. The FVC of each patient is assessed once each week to reduce leakage. To evaluate predictions, one modifies the Laplace Log Likelihood. A Confidence measure and an FVC are given to each sample in the test set (standard deviation). For each accurate FVC measurement, we provide a forecast and a level of confidence. As a result, the metric is calculated. Less than 70 confidence points cause a clip.

$$\sigma_{clipped} = \max(\sigma, 70) \quad (4.1)$$

In order to prevent big errors, errors greater than 1000 are also trimmed.

$$\delta = \min(|FVC_{true} - FVC_{predicted}|, 100) \quad (4.2)$$

Metric is defined as:

$$metric = -2\delta - \ln(\sqrt{2} * \sigma_{clipped}) \quad (4.3)$$

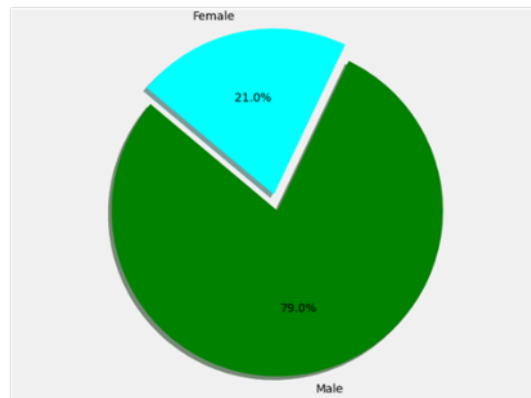


Fig. 5.1: Pie Chart for Gender Distribution

We also used different cmap models to plot CT images of some patients in order to fully understand the extent of their lung function decline. The activation function converts inputs with a given range into outputs. Sigmoid activation functions, for example, take input and map output values between 0 and 1. When enabled, Leaky ReLU provides a non-zero slope to each layer. The activation function's representation is Leaky ReLU: $F(x) = 0.01x, x \geq 0$ and $F(x) = 0, x < 0$. To segment the lung region, a deep learning model using Unet is proposed with provided promising results for the given dataset. For better training of the model, image augmentation were created using the Albumentations and also lung masks are created. Lung Masks are created for 100 CT scans images using the normalization method. The following transformations are applied:

1. Rotate the scan by 30 degrees.
2. Horizontal flip the scan
3. Grid Distortion: It is a method of warping images that relies on mapping between families of equivalent curves that are placed in grid layout
4. Elastic transform: Transform enables us to convert existing Elastic search indices into summarized indices, which provides opportunities for new insights and analytics.
5. Early stopping is also used in the segmentation model to minimize the training time and also to achieve accurate output with sufficient amount of training. The patience value in early stopping class is set to 7. To prevent overfitting during the training phase, early stopping is a type of regularisation. When model performance on a hold out validation dataset stops improving, we can provide an arbitrary large number of training epochs and end training.

Utilizing CUDA, a segmentation model is trained over 80 epochs (Nvidia's CUDA is a parallel computing platform and programming model designed for generic computing on its own GPUs). CUDA enables developers to accelerate computationally demanding programmes by utilising the capacity of GPUs for the parallelizable portion of the calculation. Batch Size (The batch size is a number of samples processed before the model is updated) is 8. We have obtained an accuracy of 92.59 percent for the proposed model after training.

5. Results and Discussion. In this study, two lung segmentation neural network architectures are investigated using two Kaggle datasets. To evaluate the model performance in this work, a dataset of 176 images from these two datasets in Kaggle is used. Fig. 5.1 depicts a pie chart for gender distribution. The chart describes that there are 79 percent of males and 21 percent of females in the given dataset. Fig.5.2 displays a plot of the patients' FVC (measured in millilitres) values using the Laplace distribution. FVC has a maximum of 6399.00, a low of 827.00, mean of 2690.48 and standard deviation of 832.77.

Fig. 5.3 depicts a pie chart for age distribution. According to the pie chart, there are more patients (51.19 percent) in the 60-70 year age group, followed by the 70-80 year age group (31.05 percent). The lowest percentage of smokers (2.78 percent) are over the age of 80. The age group under 60 years old accounts for 14.98 percent of the population. Fig. 5.4 depicts the age of all patients in the dataset using the Laplace distribution.

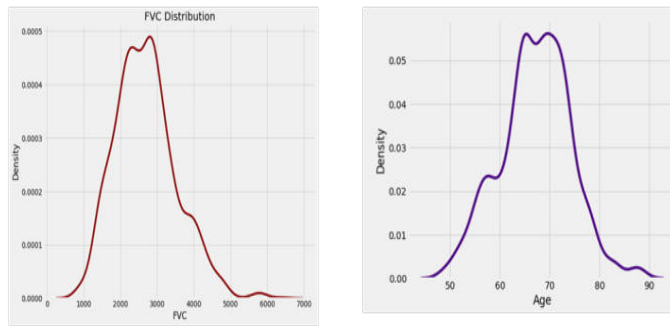


Fig. 5.2: FVC using Laplace distribution

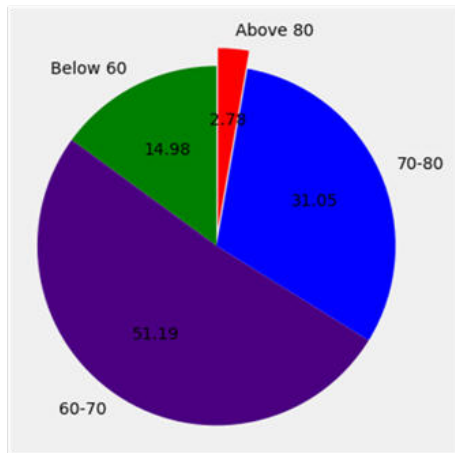


Fig. 5.3: Pie Chart for Age Distribution

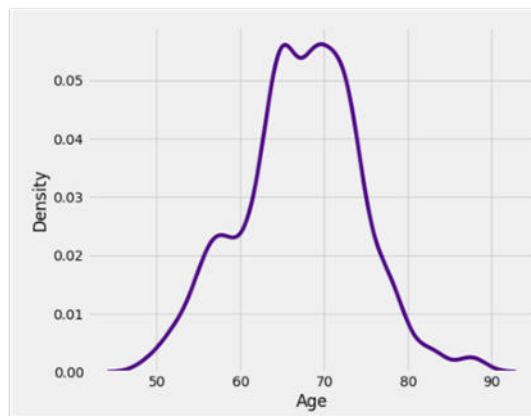


Fig. 5.4: Age based on Smoking Status

The oldest person is 88 years old, the youngest is 49 years old, the average age is 67.19 years, and the standard deviation is 7.06 years.

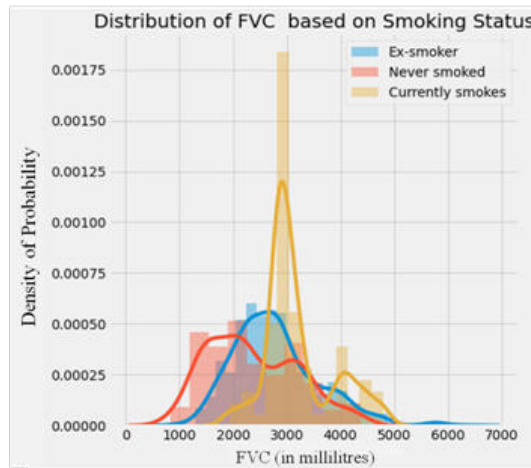


Fig. 5.5: Age plot using Laplace distribution

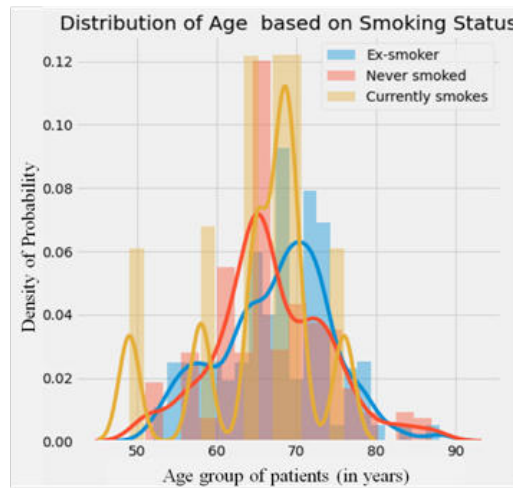


Fig. 5.6: FVC based on Smoking Status

Fig. 5.5 depicts the FVC Laplace distribution of patients and categorises them based on their smoking status (ex-smoker, never smoked, presently smokes). Fig. 5.6 displays the age distribution of patients categorized based on their smoking status (ex-smoker, never smoked, presently smokes) Figures below show the plots of multiple color map models for some patients Fig. 5.7 depicts a color map of patients' CT images in a binary model. It belongs to sequential class of color maps. Sequential color maps are basic color maps that start at a reasonably low lightness value and uniformly increase to a higher value. They are commonly used to represent information that is ordered. Fig.5.8 depicts a color map of patients' CT images in a Hot model. It belongs to sequential class of color maps.

Fig. 5.9 depicts a color map of patients' CT images in a Spectral Model. It belongs to Diverging class of color maps. Unlike sequential color maps, diverging color maps start at their lowest lightness value at both ends and monotonically/linearly increase to the highest lightness value in the center. They could be seen as two sequential color maps combined together, that share the same lightness range and end/begin with the same color. This makes them very useful to represent information that has a critical middle value. Fig. 5.10 depicts a color



Fig. 5.7: CT scans in Binary Model

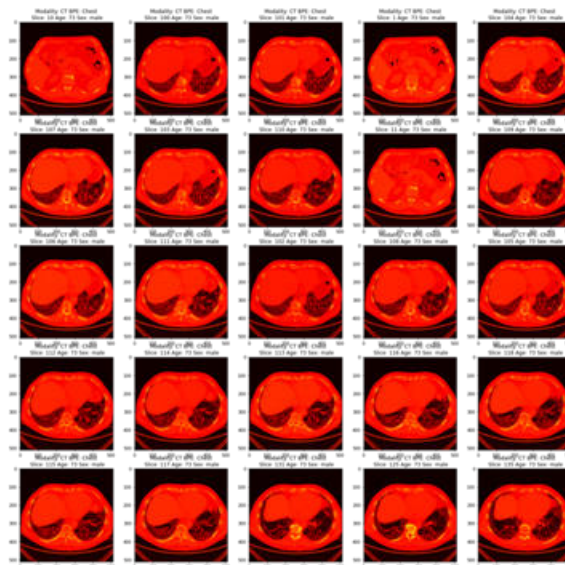


Fig. 5.8: CT scans in Hot Model

map of patients' CT images in a Seismic Model. It belongs to Diverging class of color maps. The correlation matrix is depicted in Fig. 5.10 with the parameters weeks, FVC, percent, and age. Correlation is a statistical technique used by statisticians and data analysts to study the relationships between two numerical variables. A correlation matrix is a collection of correlation coefficients between dataset attributes. A correlation value can be calculated in numerous ways. The correlation matrix is a symmetric matrices with all diagonal equal to one

Fig. 5.11 depicts a colormap of patients' CT images in a Hot model. It belongs to sequential class of colormaps. Fig. 5.12 depicts a colormap of patients' CT images in a Spectral Model. It belongs to Diverging



Fig. 5.9: CT scans in Spectral Model

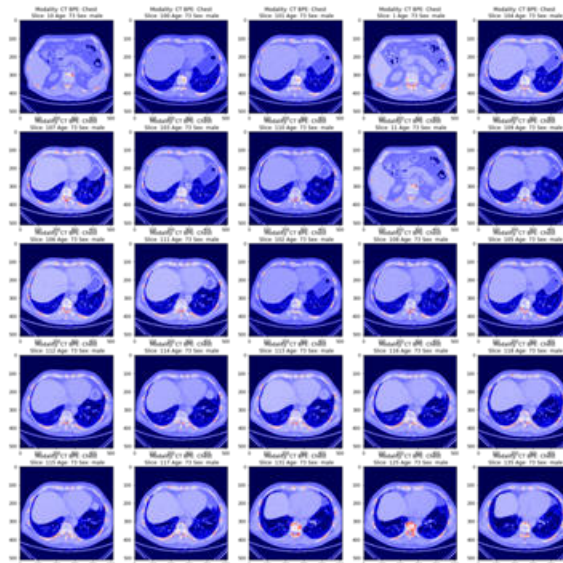


Fig. 5.10: CT scans in Seismic Model

class of colormaps. Unlike sequential colormaps, diverging colormaps start at their lowest lightness value at both ends and monotonically/linearly increase to the highest lightness value in the center. They could be seen as two sequential colormaps combined together, that share the same lightness range and end/begin with the same color. This makes them very useful to represent information that has a critical middle value.

Fig. 5.13 depicts a colormap of CT images from patients in a Seismic Model, belonging to the diverging colormap class. Correlation is used by statisticians and data analysts to investigate the correlations between two numerical variables. A correlation matrix is made up of a collection of correlation coefficients between characteristics in a dataset. A correlation value can be calculated in numerous ways. The correlation matrix is

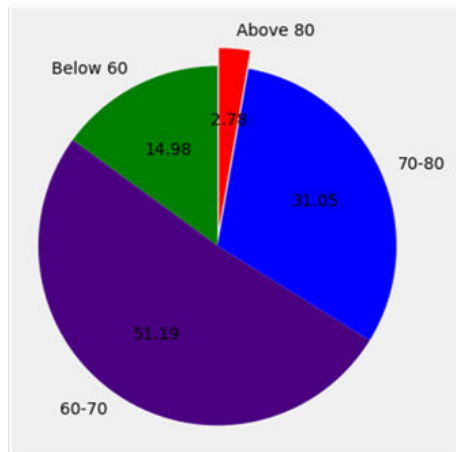


Fig. 5.11: Pie Chart for Age Distribution

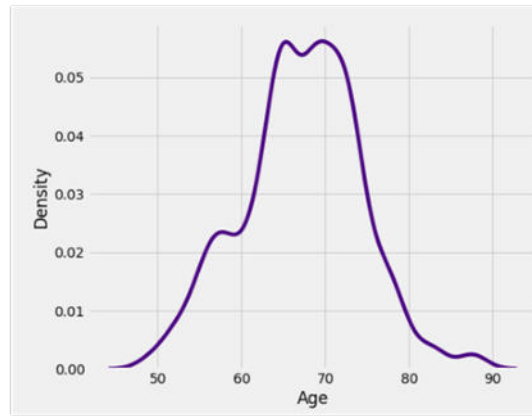


Fig. 5.12: Age plot using Laplace distribution

Table 5.1: FVC final values and patient confidence in the test folder of the presented dataset

Sl.No	Patient Id	FVC	Confidence
1	ID00419637202311204720266	2877.7510	181.3220
2	ID00421637202311550012434	2809.9716	172.7606
3	ID00422637202311677017372	2118.5655	149.2117
4	ID00423637202312137826373	3195.3938	189.5431
5	ID00426637202313170790469	2812.7246	174.9930

a symmetric matrices with all diagonal equal to one.

Fig. 5.14 depicts the correlation matrix with parameters weeks, FVC, percentage and age. The Table 5.1 describes the values of FVC and Confidence when the training dataset is fed into the trained model:

The FVC and their corresponding confidence value for the supplied dataset are found using a Python model in this work. Fig. 5.15 depicts the output of the segmentation model.

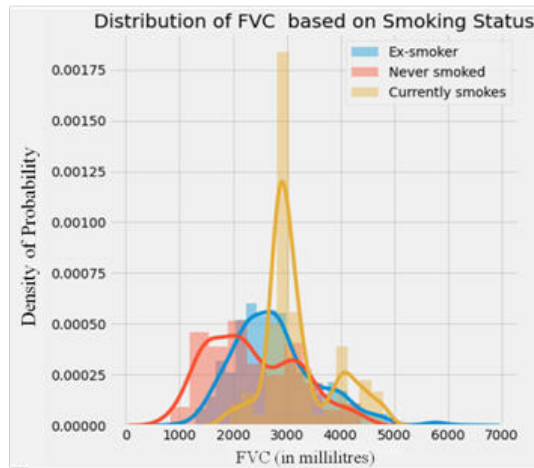


Fig. 5.13: FVC based on Smoking Status



Fig. 5.14: Correlation matrix

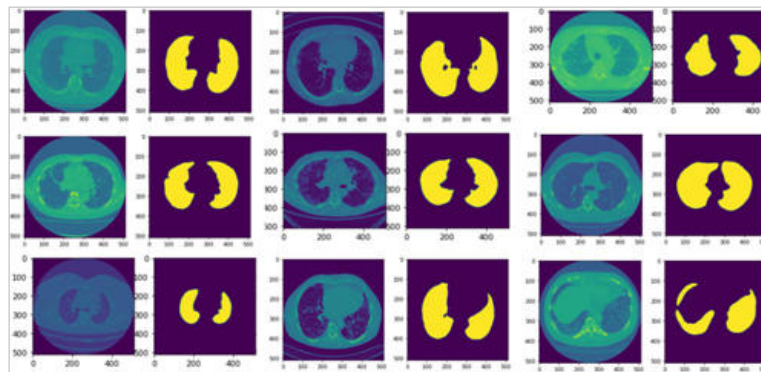


Fig. 5.15: Output of the segmentation model

6. Conclusions and future scope. In this paper, we proposed a systematic approach for ILD segmentation. The approach with the cascaded models achieved elegant performance levels in segmentation and also infection quantification. The proposed segmentation technique has proven to be very useful because it can be implemented using machine learning and deep learning techniques for lung segmentation and has garnered

impressive outcomes. The proposed system outperforms the existing systems with limited dataset images and producing effective results by attaining 92.5% accuracy. The effectiveness of the FVC and their corresponding confidence value for the supplied datasets are determined using a Python model. The stage-wise enhancement of the deep learning algorithm performance has significantly enhanced the performance of the proposed deep learning network-based ILD classifier. Using these findings, we were able to identify whether a person had a condition, allowing for an early diagnosis. When the confidence value is low, the FVC value is measured more effectively. The model network can utilize the crucial data points while suppressing the unimportant ones due to leaky ReLU and activation functions of ReLU. To better evaluate its severity, we plotted the CT image using various color map models. The application was developed using CUDA, a parallel computing environment and programming paradigm that greatly enhances computing performance by utilising the capabilities of the graphics processing unit. To further improve the diagnosis of ILD sickness, the model can be upgraded with a suitable classifier to segment the lung and identify the precise region of the lung that is infected. Deep Learning-based algorithms for fully automatic segmentation have developed as a result of the time-consuming and erroneous nature of manual and semiautomatic segmentation. When lung wall tissue patterns with thick tissue are present, the proposed model performs well.

REFERENCES

- [1] Uppaluri, Renuka, et al. "Computer recognition of regional lung disease patterns." *American journal of respiratory and critical care medicine* 160.2 (1999): 648-654.
- [2] Shen, Dinggang, Guorong Wu, and Heung-Il Suk. "Deep learning in medical image analysis." *Annual review of biomedical engineering* 19 (2017): 221-248.
- [3] Antoniou, Katerina M., et al. "Interstitial lung disease." *European Respiratory Review* 23.131 (2014): 40-54.
- [4] Raj, MR Daniya, and C. Helen Sulochana. "An efficient lung segmentation approach for interstitial lung disease." 2014 International Conference on Circuits, Power and Computing Technologies [ICCPCT-2014]. IEEE, 2014.
- [5] Devaki, K., and V. MuraliBhaskaran. "Study of computed tomography images of the lungs: A survey." 2011 International Conference on Recent Trends in Information Technology (ICRTIT). IEEE, 2011.
- [6] Russakovsky, Olga, et al. "Imagenet large scale visual recognition challenge." *International journal of computer vision* 115.3 (2015): 211-252.
- [7] LeCun, Yann, et al. "Gradient-based learning applied to document recognition." *Proceedings of the IEEE* 86.11 (1998): 2278-2324.
- [8] Greenspan, Hayit, Bram Van Ginneken, and Ronald M. Summers. "Guest editorial deep learning in medical imaging: Overview and future promise of an exciting new technique." *IEEE transactions on medical imaging* 35.5 (2016): 1153-1159.
- [9] Beichel, Reinhard. "Model-Based Segmentation of Pathological Lungs in Volumetric CT Data."
- [10] Hamzah, Mohd Faizal Mohd, et al. "Detection of interstitial lung disease using correlation and regression methods on texture measure." 2017 IEEE International Conference on Imaging, Vision and Pattern Recognition (icIVPR). IEEE, 2017.
- [11] Mandal, Sampurna, et al. "Prediction analysis of idiopathic pulmonary fibrosis progression from OSIC dataset." 2020 IEEE International conference on computing, power and communication technologies (GUCON). IEEE, 2020.
- [12] Hattikatti, Pratiksha. "Texture based interstitial lung disease detection using convolutional neural network." 2017 International Conference on Big Data, IoT and Data Science (BIGDATA). IEEE, 2017.
- [13] Heitmann, K. R., et al. "Automatic detection of ground glass opacities on lung HRCT using multiple neural networks." *European radiology* 7.9 (1997): 1463-1472.
- [14] Demedts, M., and U. Costabel. "ATS/ERS international multidisciplinary consensus classification of the idiopathic interstitial pneumonias." (2002): 794-796.
- [15] Xu, Ye, et al. "Computer-aided classification of interstitial lung diseases via MDCT: 3D adaptive multiple feature method (3D AMFM)." *Academic radiology* 13.8 (2006): 969-978.
- [16] Korfiatis, Panayiotis D., et al. "Texture-based identification and characterization of interstitial pneumonia patterns in lung multidetector CT." *IEEE transactions on information technology in biomedicine* 14.3 (2009): 675-680.
- [17] Gangeh, Mehrdad J., et al. "A texton-based approach for the classification of lung parenchyma in CT images." International conference on medical image computing and computer-assisted intervention. Springer, Berlin, Heidelberg, 2010.
- [18] Xu, Rui, et al. "Classification of diffuse lung disease patterns on high-resolution computed tomography by a bag of words approach." International Conference on Medical Image Computing and Computer-Assisted Intervention. Springer, Berlin, Heidelberg, 2011.
- [19] Depeursinge, Adrien, et al. "Near-affine-invariant texture learning for lung tissue analysis using isotropic wavelet frames." *IEEE Transactions on Information Technology in Biomedicine* 16.4 (2012): 665-675.
- [20] Loarce-Martos, Jesus, Francisco Xavier Leon-Roman, and Sandra Garrote-Corral. "Recent advances in quantitative computerized tomography and home spirometry for diagnosing and monitoring of interstitial lung disease associated with connective tissue diseases: A narrative review." (2021).
- [21] Rehman, Aasia, Muheet Ahmed Butt, and Majid Zaman. "A Survey of Medical Image Analysis Using Deep Learning Ap-

- proaches." 2021 5th International Conference on Computing Methodologies and Communication (ICCMC). IEEE, 2021.
- [22] Hua, Panfang. Segmentation of lung tissue in CT images with disease and pathology. Diss. The University of Iowa, 2010.
- [23] Tolouee, Azar, et al. "Image based diagnostic aid system for interstitial lung diseases." *Expert Systems with Applications* 38.6 (2011): 7755-7765.
- [24] Gomathi, M., and P. Thangaraj. "A new approach to lung image segmentation using fuzzy possibilistic C-means algorithm." *arXiv preprint arXiv:1004.1768* (2010).
- [25] Sluimer, Ingrid, Mathias Prokop, and Bram Van Ginneken. "Toward automated segmentation of the pathological lung in CT." *IEEE transactions on medical imaging* 24.8 (2005): 1025-1038.
- [26] Pawar, Swati P., and Sanjay N. Talbar. "Two-Stage Hybrid Approach of Deep Learning Networks for Interstitial Lung Disease Classification." *BioMed Research International* 2022 (2022).
- [27] Reddy, N. Sudhir, and V. Khanaa. "LDDC-Net: Deep Learning Convolutional Neural Network-based lung disease detection and classification." *JOURNAL OF ALGEBRAIC STATISTICS* 13.1 (2022): 526-542.
- [28] Ravi, Vinayakumar, Vasundhara Acharya, and Mamoun Alazab. "A multichannel EfficientNet deep learning-based stacking ensemble approach for lung disease detection using chest X-ray images." *Cluster Computing* (2022): 1-23.
- [29] Nandy, Sreyankar, et al. "Deep learning-based automated, high-throughput microscopic assessment of interstitial lung disease using endobronchial optical coherence tomography." *Optical Coherence Tomography and Coherence Domain Optical Methods in Biomedicine XXVI. SPIE*, 2022.
- [30] Kihira, Shingo, et al. "U-Net Based Segmentation and Characterization of Gliomas." *Cancers* 14.18 (2022): 4457.
- [31] Agarwal, Mohit, et al. "Eight pruning deep learning models for low storage and high-speed COVID-19 computed tomography lung segmentation and heatmap-based lesion localization: A multicenter study using COVLIAS 2.0." *Computers in Biology and Medicine* (2022): 105571.
- [32] Siddiquee, Sadi Mohammad, et al. "COVID-19 Severity Prediction from Chest X-ray Images using an Anatomy-Aware Deep Learning Model." (2022)
- [33] Wang, Risheng, et al. "Medical image segmentation using deep learning: A survey." *IET Image Processing* 16.5 (2022): 1243-1267.
- [34] Walsh, Simon LF, et al. "Deep learning-based outcome prediction in progressive fibrotic lung disease using high-resolution computed tomography." *American journal of respiratory and critical care medicine* ja (2022).
- [35] Ji, Jiarui, et al. "Automated Vein Segmentation from NIR Images Using a Mixer-UNet Model." *International Conference on Intelligent Robotics and Applications. Springer, Cham*, 2022.
- [36] Ghali, Rafik, and Moulay A. Akhloufi. "ARSeg: An Attention RegSeg Architecture for CXR Lung Segmentation." *2022 IEEE 23rd International Conference on Information Reuse and Integration for Data Science (IRI). IEEE*, 2022.
- [37] Ahmed, Imran, Abdellah Chehri, and Gwanggil Jeon. "A Sustainable Deep Learning-Based Framework for Automated Segmentation of COVID-19 Infected Regions: Using U-Net with an Attention Mechanism and Boundary Loss Function." *Electronics* 11.15 (2022): 2296.
- [38] Bassi, Pedro RAS. "ISNet: Costless and Implicit Image Segmentation for Deep Classifiers, with Application in COVID-19 Detection." *arXiv preprint arXiv:2202.00232* (2022).
- [39] Chhabra, Mohit, and Rajneesh Kumar. "A Smart Healthcare System Based on Classifier DenseNet 121 Model to Detect Multiple Diseases." *Mobile Radio Communications and 5G Networks. Springer, Singapore*, 2022. 297-312.
- [40] Inan, Muhammad Sakib Khan, Fahim Irfan Alam, and Rizwan Hasan. "Deep integrated pipeline of segmentation guided classification of breast cancer from ultrasound images." *Biomedical Signal Processing and Control* 75 (2022): 103553

Edited by: Vinoth Kumar

Received: Aug 23, 2022

Accepted: Nov 7, 2022